Dispersion properties of inhomogeneous nanostructures

Uriel Levy and Yeshaiahu Fainman

Department of Electrical and Computer Engineering, University of California, San Diego, 9500 Gilman Drive, La Jolla, California 92093-0407

Received October 10, 2003; revised manuscript received December 16, 2003; accepted December 18, 2003

We analyze the dispersive properties of inhomogeneous nanostructures (INSs) composed of alternating layers of different materials. Analysis of the interaction between the propagating pulse and the INS provides modified dispersion characteristics. An approximate theoretical model predicting the dispersion properties of the INS is developed and compared with more accurate numeric computation results. It is shown that the dispersion coefficient can be engineered by controlling the spatial distribution of the pulse carrier, the geometry of the INS, and the refractive indices of the materials combined to construct the INS. Specifically, the dispersion coefficient can be engineered to yield various types of dispersion, including normal dispersion, anomalous dispersion, and zero dispersion. As such, the discussed INS can be useful for applications that will benefit from engineered dispersion management and control. © 2004 Optical Society of America

OCIS codes: 050.2770, 070.2580, 260.5430, 350.5500.

1. INTRODUCTION

The spectral dispersion phenomenon is one of the key factors limiting the transmission bandwidth in optical communication systems. Dispersion causes each spectral component of the optical pulse to propagate with a slightly different group velocity, resulting in a pulse broadening. Commonly, dispersion effects are discussed in the context of pulse propagation over a long distance within an optical fiber. However, with recent advances toward ultrahigh-bandwidth transmission, shorter pulses are being used,[1–4] and dispersion issues can no longer be considered negligible, even for propagation over short distances.

Dispersion management and control in modern communication systems have motivated a number of research efforts toward development of dispersion management techniques and devices, such as chirped Bragg gratings,[5] dispersion-compensating fibers (e.g., systems composed of alternating sections of positive and negative dispersive media),[6] and dispersion-shifted fibers.[7] Dispersion can also be controlled by use of a free-space setup, such as the achromatic Fourier transformer.[8] Another approach for engineering the dispersion properties is cascading a large number of all-pass filters [9], providing a desired group velocity versus frequency dependence. One of the possible realizations of such devices can be implemented with microresonators.[10] A summary of various dispersion management techniques can be found in Ref. 11.

Typically, the analysis of pulse propagation in a guiding media involves three major dispersion mechanisms:[12] material dispersion, waveguide dispersion (i.e., the dispersion of a specific mode), and modal dispersion (i.e., the dispersion caused by the different group velocity for each mode). Equivalently, one can analyze the free-space propagation of a pulse within a nonguiding dielectric media by decomposing the spatial distribution of a single pulse into its Fourier spectral components in space and time (in the case of a pulse train, obtained by use of a mode-locked source, the pulse should be convolved with a comb function in time). Each spatial-frequency Fourier component can be considered a free-space spatial mode with one major distinction: There is a continuum of free-space modes, whereas waveguide modes are discrete. Similar to waveguide modes, the dispersion analysis of these continuous modes should take into account material dispersion, waveguide-type dispersion, and modal dispersion. Moreover, one can think of a special theoretical case for free space, in which only a single mode is propagating through the nonguiding media, similar to single-mode waveguides. One example is the propagation of a pulse carried by a nondiffracting Bessel beam in space. The propagation of such a beam in free space and in a nonguiding dielectric media was already analyzed.[13–19] Other examples are the propagation of a pulse carried by a plane wave or by a standing cosine beam in space. The cosine beam is of special interest, since, as an eigenmode of the wave equation (in Cartesian coordinates), it can also be considered an example of a nondiffracting beam.

In this paper we investigate the dispersion properties of nonresonant inhomogeneous nanostructures (INSs), which allow the free-space propagation of a pulse for dispersion management and control purposes. In the past, such structures have been engineered to create unique anisotropic properties.[20–24] These nonresonant INSs, commonly composed of one-dimensional subwavelength periodic structures, are characterized by an effective refractive index usually different for the TE and the TM polarization states of the optical fields. As such, INS-based elements have been used as birefringent wave plates as well as polarization converters.[25]

An approximate analysis of these INSs can be performed with the effective medium theory (EMT).[26] For higher-accuracy analysis, more complex approaches can be used including rigorous coupled-wave analysis[27]

(RCWA), the finite-difference time domain,[28] the boundary- element method,[29] or the finite-element method.[30]

Although zero-order EMT predicts that the effective refractive index is not wavelength dependent (neglecting the intrinsic material dispersion), this assumption is valid only for an INS having a period much smaller than the wavelength of the optical wave. As the period becomes close to the wavelength of the optical wave, the effective index is becoming wavelength dependent as evident from EMT that includes terms higher than zero order, thus modifying the dispersion properties of the INS. We will refer to this phenomenon as a structural dispersion. For example, broadband-retardation wave plates[31,32] were constructed utilizing the structural dispersion in subwavelength periodic structures.

Recently it has been shown that engineering the dispersion properties of a fiber can be achieved by use of the so-called holy fibers.[33] These structures allow control of the effective index of the fiber, its propagation constant, dispersion properties, and nonlinearities. Similarly, one can think of periodic bulk optical elements, composed of alternating layers of different materials and having a period smaller than the wavelength of light with propagation direction of optical fields in the plane of the layers (see Fig. 1), such that no diffraction harmonics (besides the zero order) can propagate through the material. Although the realization of such composite materials is currently challenging, these fabrication challenges may be overcome with the rapid advance in nanotechnology and developing nanofabrication techniques.

In Section 2 we review free-space propagation of a continuum of spatial modes and their analogy to waveguide modes. In particular, we discuss the case of a single-mode illumination of an INS, in which the analysis of pulse propagation is somewhat equivalent to the analysis of a pulse propagating within a single-mode waveguide and having no modal dispersion. Two such cases are presented in Sections 3 and 4. In Section 3 we evaluate the dispersion coefficient of an optical pulse carried by a plane wave and propagating within the INS. On the basis of the second-order EMT, we present an approximate model capable of predicting the structural dispersion coefficient. This model is followed by more accurate analysis based on RCWA. Intrinsic material dispersion and structural dispersions, and their combined effects, are analyzed and discussed. In Section 4 we extend this discussion by evaluating the dispersion coefficient for the case of a pulse carried by a standing cosine wave in space and propagating within the INS. For such a beam, the propagation constant and the corresponding wave number are different, such that the waveguide-type dispersion needs also to be considered. We show that by proper choice of parameters the combination of intrinsic material dispersion, structural dispersion, and waveguide-type dispersion can produce almost any desired dispersion characteristics, leading to various INS-based potential devices that are very useful for dispersion management and control. Conclusions and final discussions are summarized in Section 5.

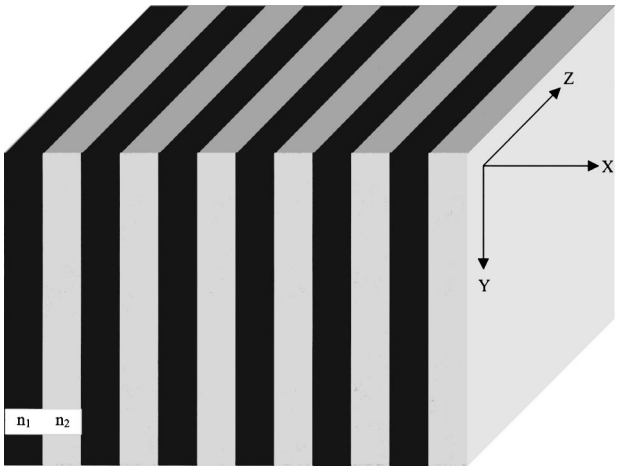

Fig. 1. Schematic diagram of the INS geometry.

2. CONTINUUM OF MODES IN FREE SPACE

Consider an incident optical pulse with an envelope $h(t)$ propagating along the optical axis in the z direction and, for simplicity, having a one-dimensional transverse spatial distribution (along the x axis). In the plane of incidence ($z = 0$) the field distribution is given by

$$E(x, z = 0, t) = \int_{-\infty}^{\infty} \bar{E}(x, z = 0, \omega)\exp[j(\omega - \omega_0)t]\mathrm{d}\omega, \tag{1}$$

where ω_0 is the carrier frequency and $\bar{E}(x, z = 0, \omega)$ describes the transverse spatial distribution of the temporal spectrum of the incident field, obtained by plane-wave spectrum decomposition,[34]

$$\begin{aligned}\bar{E}(x, z = 0, \omega) &= \int_{-\infty}^{\infty} A(f_x, z = 0)\exp(j2\pi f_x x)H(\omega)\mathrm{d}f_x \\ &= \int_{-\infty}^{\infty} U(f_x, z = 0, \omega)\exp(j2\pi f_x x)\mathrm{d}f_x,\end{aligned} \tag{2}$$

where $A(f_x, z = 0)$ is the spatial plane-wave spectrum and $H(\omega)$ is the Fourier transform of the temporal envelope $h(t)$ of the incident pulse waveform.

Next, we calculate the field distribution at a distance z, obtaining

$$\begin{aligned}\bar{E}(x, z, \omega) &= \int_{-\infty}^{\infty} A(f_x, z)\exp(j2\pi f_x x)H(\omega)\mathrm{d}f_x \\ &= \int_{-\infty}^{\infty} U(f_x, z, \omega)\exp(j2\pi f_x x)\mathrm{d}f_x.\end{aligned} \tag{3}$$

Since $\bar{E}(x, z, \omega)$ must obey the wave equation,[34]

$$\left[\frac{\partial^2}{\partial x^2} + \frac{\partial^2}{\partial z^2} + K(\omega)^2\right]\bar{E}(x, z, \omega) = 0. \tag{4}$$

Substitution of Eq. (3) into Eq. (4) yields

$$U(f_x, z, \omega) = U(f_x, z = 0, \omega)\exp(j\beta z), \tag{5}$$

where the propagation constant is given by

$$\beta = [K^2(\omega) - 4\pi^2 f_x^2]^{1/2}. \tag{6}$$

The spatial frequency f_x is related to the angular frequency (i.e., the propagation angle of each plane wave) by[34]

$$2\pi f_x = K(\omega)\sin(\theta) = \alpha, \tag{7}$$

where $K(\omega)$ is the wave number and θ is the tilt angle of the plane wave, measured from the z axis. The propagation constant is thus given by

$$\beta(\omega) = [K^2(\omega) - K^2(\omega)\sin^2(\theta)]^{1/2} = [K^2(\omega) - \alpha^2]^{1/2} = K(\omega)\cos(\theta) = \frac{\omega}{C} n\cos(\theta) = \frac{2\pi\nu}{C} n\cos(\theta), \tag{8}$$

where n is the refractive index and c is the speed of light in vacuum.

Additional simplification can be obtained by assuming a symmetric spectrum, i.e., $A(f_x) = A(-f_x)$, yielding

$$\bar{E}(x, z, \omega) \propto 2\int_{0^+}^{\infty} U(\alpha, 0, \omega)\exp[j\beta(\omega)z] \times \cos(\alpha x)\mathrm{d}\alpha + U(0, 0, \omega)\exp[jK(\omega)z]. \tag{9}$$

As can be seen, expression (9) describes a continuum of cosine waves in space, each having a different spatial frequency (α or f_x) and a different propagation constant (β), and each is multiplied by a weighting factor $U(\alpha, 0, \omega)$. Expression (9) is analogous to the description of modes propagating within a symmetrical multimode waveguide, with one important distinction: Waveguide modes contain only a discrete and finite set, whereas free-space modes are continuous and infinite. However, if we construct a discrete set of spatial frequencies, i.e.,

$$U(\alpha, 0, \omega) = \sum_{n=1}^{N} U(\alpha_n, 0, \omega)\delta(\alpha - \alpha_n), \tag{10}$$

with $\delta(x)$ as a Dirac delta function, expression (9) will take the form

$$\bar{E}(x, z, \omega) \propto \sum_{n=1}^{N} U(\alpha_n, 0, \omega)\exp[j\beta_n(\omega)z]\cos(\alpha_n x), \tag{11}$$

and the analysis of a pulse propagating in the INS will become somewhat similar to that in a multimode fiber.

As a special case, we now consider free-space propagation of a single spatial mode:

$$\bar{E}(x, z, \omega) \propto U(\alpha, 0, \omega)\exp[j\beta(\omega)z]\cos(\alpha x). \tag{12}$$

Such a field distribution can be created by the interference of two tilted plane waves ($\alpha \neq 0$) or by use of a single plane-wave illumination along the optical axis ($\alpha = 0$). Although a pure plane wave is only a mathematical definition since it carries infinite energy, it can be approximated by use of a large aperture with diameter D, as long as the propagation distance is small enough to satisfy the inequality $z < D^2/\lambda$, where D is the aperture size.

Commonly, the propagation constant's dependence on the temporal spectrum can be described with a Taylor-series expansion:

$$\beta(\omega) \approx \beta(\omega_0) + \beta'(\omega_0)(\omega - \omega_0) + \frac{1}{2}\beta''(\omega_0)(\omega - \omega_0)^2 + \ldots = \beta(\nu_0) + \frac{2\pi}{V_g}(\nu - \nu_0) + \pi D_\nu(\nu - \nu_0)^2, \tag{13}$$

where we defined the group velocity as

$$\frac{1}{V_g} = \frac{1}{2\pi}\frac{\mathrm{d}\beta}{\mathrm{d}\nu}\bigg|_{\nu_0} = \frac{\mathrm{d}\beta}{\mathrm{d}\omega}\bigg|_{\omega_0} \tag{14}$$

and the group-velocity dispersion (the linear dispersion coefficient) as

$$D_\nu = \frac{1}{2\pi}\frac{\mathrm{d}^2\beta}{\mathrm{d}\nu^2}\bigg|_{\nu=\nu_0} = 2\pi\frac{\mathrm{d}^2\beta}{\mathrm{d}\omega^2}\bigg|_{\omega=\omega_0} = \frac{\mathrm{d}}{\mathrm{d}\nu}\left(\frac{1}{V_g}\right)_{\nu=\nu_0}, \tag{15}$$

with $\nu = \omega/2\pi$ and ν_0 representing the carrier frequency. As shown elsewhere,[19] higher-order dispersion terms can be neglected as long as the pulse width is more than few optical cycles.

By substituting expression (13) and Eqs. (14) and (15) into expression (11), we obtain the well-known temporal frequency transfer function

$$\bar{E}(x, z, \nu) \propto H_0(\nu)\exp[j\beta(\nu_0)z]\exp[j2\pi z(\nu - \nu_0)/V_g] \times \exp[j\pi D_\nu z(\nu - \nu_0)^2]. \tag{16}$$

The exponential containing the inverse of the group velocity represents a linear phase shift in frequency, corresponding to a delay in the time domain, $\tau = z/V_g$. In general, the group velocity will be different for each spatial-frequency mode, resulting in modal dispersion, modifying the temporal shape of the pulse, except for a single-mode case as discussed above. Thus, for a single spatial mode field, the group-velocity term does not affect the waveform shape of the temporal pulse. In contrast, the second exponential term containing the dispersion coefficient is a quadratic phase factor, resulting in chirping the spectrum in the time domain, thus leading to stretching of the waveform of the original pulse (assuming that the incident pulse is transform limited). Next, we will investigate propagation of such single-mode fields in INS materials.

3. PROPAGATION OF A PULSED PLANE WAVE IN INHOMOGENEOUS NANOSTRUCTURE MEDIA

In this section we analyze the dispersion properties of a nonguiding media made of an INS consisting of alternating layers made of materials with different refractive indices in the x direction and infinite in the y direction. The incident pulse propagates along the z axis, perpendicular to the k vector of the INS, as shown schematically in Fig. 1. Throughout the analysis we assume a transform-limited temporal pulse carried by a single spatial-frequency plane wave propagating in the INS. As discussed above, the propagation of such a pulse is

equivalent to the propagation of the ground-state mode ($\alpha = 0$). The temporal Fourier transform of the field distribution is given by

$$\bar{E}(x, z, \nu) = H_0(\nu)\exp[j\beta(\nu)z] = H_0(\nu)\exp jK(\nu)z, \tag{17}$$

where

$$U(\alpha, 0, \nu) = \begin{Bmatrix} H(\nu) & \alpha = 0 \\ 0 & \text{otherwise} \end{Bmatrix} \tag{18}$$

and $K(\nu) = \beta(\nu)$.

Since $K = \beta$, the dispersion coefficient is proportional only to the second derivative of K [see Eq. (15)]. As such, only effective material dispersion is expected to play a role, since waveguide-type and modal dispersion mechanisms do not exist. However, evaluating the material dispersion is not straightforward, since the composite material is represented by an effective refractive index, which is dependent on both optical frequency and polarization state, as was already mentioned by several authors.[35] For INS material the dispersion characteristics are modified by structural dispersion representing the interaction of the vector optical field with the composite nanostructure.

On the basis of the second-order EMT,[26] we next describe a simple model allowing us to predict the dispersion coefficient of the INS and to achieve better understanding of the relations between the structural parameters and the corresponding dispersion properties. As a first step, we focus our interest on the structural dispersion (i.e., the dispersion due to the layered structure) and ignore the intrinsic dispersion of each constituent material. The model accuracy is later examined by comparison with more accurate results obtained from using RCWA. The accuracy of this analysis is further enhanced by accounting for the intrinsic material dispersion.

The second-order EMT provides the refractive indices for the TE ($E = E\hat{y}$) and the TM ($H = H\hat{y}$) polarization states:

$$n_{\mathrm{TE}}^{(2)} = \left\{ [n_{\mathrm{TE}}^{(0)}]^2 + \frac{1}{3}\left[\frac{\mathrm{d}}{\lambda}\pi f(1-f)(n_1^2 - n_2^2)\right]^2 \right\}^{1/2}, \tag{19}$$

$$n_{\mathrm{TM}}^{(2)} = \left([n_{\mathrm{TM}}^{(0)}]^2 + \frac{1}{3}\left\{ \frac{\mathrm{d}}{\lambda}\pi f(1-f)\left(\frac{1}{n_1^2} - \frac{1}{n_2^2}\right) n_{\mathrm{TE}}^{(0)} \times [n_{\mathrm{TM}}^{(0)}]^3 \right\}^2 \right)^{1/2}, \tag{20}$$

where n_1, n_2 are the refractive indices of the two materials used to construct the INS, f is the duty cycle, λ is the wavelength, d is the period of the structure, and $n_{\mathrm{TE}}^{(0)}, n_{\mathrm{TM}}^{(0)}$ are the effective indices predicted by the zeroth-order EMT for TE and TM polarization states, given by

$$n_{\mathrm{TE}}^{(0)} = [fn_1^2 + (1-f)n_2^2]^{1/2},$$

$$n_{\mathrm{TM}}^{(0)} = \frac{n_1 n_2}{[fn_2^2 + (1-f)n_1^2]^{1/2}}. \tag{21}$$

By using the following definitions,

$$\eta_{\mathrm{TE}} = \frac{\mathrm{d}\pi f(1-f)(n_1^2 - n_2^2)}{c\sqrt{3}},$$

$$\eta_{\mathrm{TM}} = \frac{\mathrm{d}\pi f(1-f)\left(\frac{1}{n_1^2} - \frac{1}{n_2^2}\right) n_{\mathrm{TE}}^{(0)}[n_{\mathrm{TM}}^{(0)}]^3}{c\sqrt{3}}, \tag{22}$$

with c as the speed of light, we obtain

$$n_j^{(2)} = \{[n_j^{(0)}]^2 + [\eta_j \nu]^2\}^{1/2}, \tag{23}$$

where j stands for TE or TM and ν is the optical frequency.

Assuming $\eta_j \nu \ll 1$, the effective indices can be rewritten by use of a Taylor expansion:

$$n_j^{(2)} \cong n_j^{(0)} + \frac{\eta_j^2 \nu^2}{2n_j^{(0)}}. \tag{24}$$

Substituting the above relations into Eqs. (14) and (15) and keeping in mind that $K(\nu) = \beta(\nu)$, we obtained analytic expressions for the group velocity V_g and the linear dispersion coefficient D_ν, respectively:

$$V_g^{(j)} = 2n_j^{(0)} \frac{c}{2[n_j^{(0)}]^2 + 3(\eta_i \nu_0)^2}, \tag{25}$$

$$D_\nu^j = \frac{3\eta_j^2}{cn_j^{(0)}}\nu_0, \tag{26}$$

where ν_0 is the carrier frequency. It is common to define a modified dispersion coefficient, D_λ, in terms of wavelength by use of the relation $D_\lambda \mathrm{d}\lambda = D_\nu \mathrm{d}\nu$, yielding

$$D_\lambda = -\frac{\nu^2}{c} D_\nu = -\frac{3\eta_j^2}{n_j^{(0)}}\frac{c}{\lambda^3}. \tag{27}$$

Defining $\Delta = n_1^2 - n_2^2$ and examining Eqs. (22) and (26), we observe that the linear dispersion coefficient is proportional to d^2, Δ^2, and $[f(1-f)]^2$ (leading to a maximal dispersion value for $f = 0.5$). We also notice that D_ν is always positive (D_λ is always negative), meaning that the structural dispersion is always normal. As a result, the total combined dispersion (both intrinsic material and structural dispersions) is expected to be larger (in absolute values) than the structural dispersion if materials having a normal intrinsic dispersion are used. On the other hand, for a case in which materials with anomalous dispersion are structured to construct an INS, the total dispersion is expected to be reduced, and might even be engineered to cancel out, since the intrinsic material dispersion and the structural dispersion will have opposite signs.

Throughout the analysis, we assumed that higher dispersion terms are negligible. We will now examine this assumption by estimating the next (cubic) dispersion term, given by

$$\exp[j\pi z\beta_3(\nu - \nu_0)^2/3], \tag{28}$$

where β_3 is the cubic dispersion coefficient given by

$$\beta_3 = \frac{1}{2\pi}\frac{\partial^3\beta}{\partial\nu^3}\bigg|_{\nu=\nu_0} = \frac{3\eta_j^2}{cn_j^{(0)}}. \tag{29}$$

By defining the effective dispersion length as the distance resulting in a π phase shift on the corresponding exponential term, we obtain

$$L_2 = (2\pi)^2\frac{T^2}{D_\nu}, \tag{30}$$

$$L_3 = 3(2\pi)^3\frac{T^3}{\beta_3}, \tag{31}$$

where T is the initial pulse duration. The dispersion length ratio is thus given by

$$L_3/L_2 = 6\pi T/\nu_0. \tag{32}$$

Therefore, as long as the pulse duration is larger than few optical cycles, the cubic dispersion term can be neglected.

As an example, we consider a structure made of alternating layers of GaAs and air. For example, such a structure can be realized by etching a subwavelength grating into a GaAs substrate with a large aspect ratio (currently, few micrometers in depth have been achieved for operation at a wavelength of 1.55 μm). At that wavelength, the refractive index of the GaAs is 3.37. Neglecting the intrinsic material dispersion, we calculate the dispersion coefficient versus the normalized period for the two principal linear polarization states by using Eq. (27) (see the solid curve in Fig. 2). To evaluate the accuracy of the suggested model, we obtained more accurate structural dispersion values by use of the RCWA approach. We obtained these results by employing the following procedure: The RCWA algorithm is applied over a limited wavelength span around the working wavelength of 1.55 μm, yielding the propagation constant for each wavelength (notice that for a low period-to-wavelength ratio only a single nonvanishing propagation constant exists). The refractive index is then calculated with Eq. (8). Once the refractive index versus wavelength (or frequency) is determined, we can perform a polynomial fit of the effective refractive index, calculate its derivatives, and find the dispersion coefficient with Eq. (15). The results are shown by the dashed–dotted curve in Fig. 2.

For comparison purposes, we also added a horizontal line, representing the intrinsic bulk material dispersion of GaAs. This value can be calculated with the Sellmeier equation[36]:

$$n^2 - 1 = \sum_{i=1}\frac{A_i\lambda^2}{\lambda^2 - \lambda_i^2}. \tag{33}$$

For GaAs, with coefficients[36] $A_1 = 2.5$, $A_2 = 7.4969$, $A_3 = 1.9347$, $\lambda_1 = 0$, $\lambda_2 = 0.4082$, and $\lambda_3 = 37.17$, we obtained a dispersion coefficient value $D_\lambda = 1230$ [picoseconds per (kilometer times nanometer)] (at $\lambda = 1.55$ μm).

From Fig. 2 we notice that the accuracy of the suggested model is very good as long as $d/\lambda < 1/10$. Beyond this value, higher-order terms of EMT need to be considered.

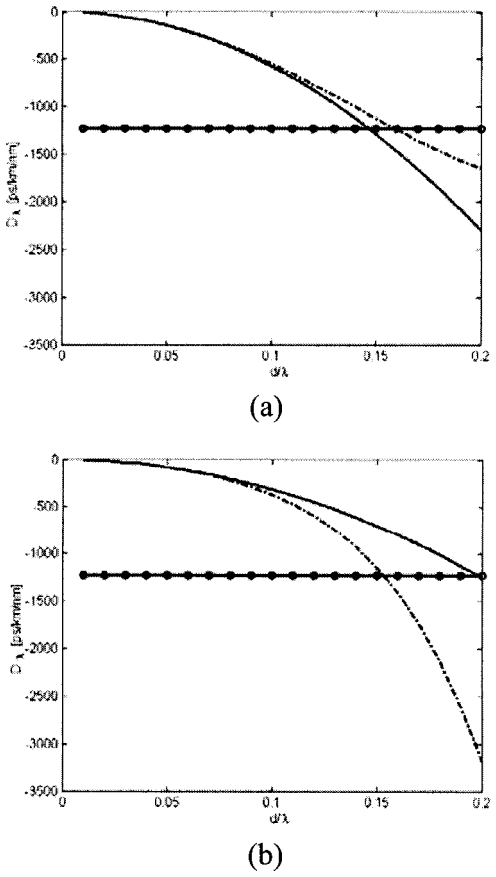

Fig. 2. Structural linear dispersion coefficient versus d/λ in a GaAs–air periodic structure (fill factor, $f = 0.5$) for (a) TE and (b) TM polarization states. Solid curve, EMT model; dashed–dotted curve, accurate results from use of RCWA; horizontal line, inherent material dispersion. [ps/km/nm], [picoseconds per (kilometer times nanometer)].

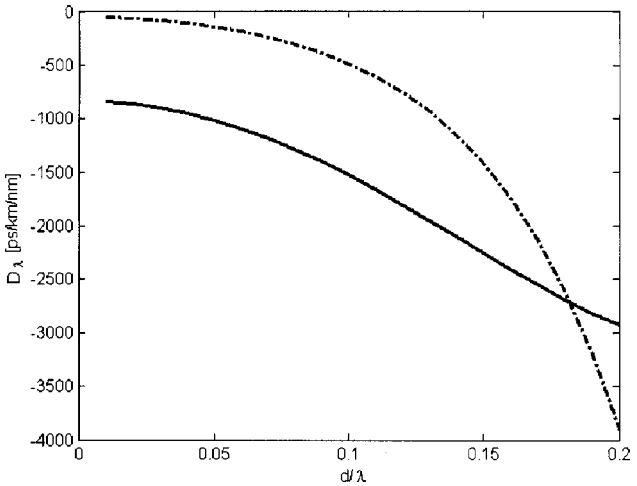

Fig. 3. Total linear dispersion coefficient versus d/λ in a GaAs–air periodic structure (fill factor $f = 0.5$) for TE (solid curve) and TM (dashed–dotted curve) polarization states.

Next, we calculate the total dispersion, combining both the structural and the intrinsic material dispersion effects (see Fig. 3). We notice that for small period-to-wavelength ratios, at which the structural dispersion is negligible, the total dispersion is reduced compared with

the dispersion in the bulk GaAs material. This result is anticipated, since one would expect the dispersion coefficient of an INS with a small period-to-wavelength ratio to be somewhere between the dispersion coefficients of the two materials used to construct the INS (in this case, the air is modeled as a nondispersive medium). It should be noted that, owing to the difference in the boundary conditions for TE- and TM-polarized fields, we expect that at low period-to-wavelength ratios, at which structural dispersion is negligible, the TM dispersion coefficient will be much smaller compared with that of the TE, since the TM-polarized field is mostly localized in the air, whereas the TE-polarized field is distributed in both air and GaAs.[37] Another explanation is based on the zero-order EMT [Eq. (3)]. By taking the derivative of the effective index with respect to the material refractive index, one obtains (assuming a duty ratio of 50% and indices of 3.37 and 1 for GaAs and air, respectively)

$$\frac{\mathrm{d}n_{\mathrm{TE}}}{\mathrm{d}n} = \frac{n}{[2(n^2+1)]^{1/2}} = 0.678,$$

$$\frac{\mathrm{d}n_{\mathrm{TM}}}{\mathrm{d}n} = \frac{1}{\sqrt{2}(n^2+1)^{3/2}} = 0.0163. \qquad (34)$$

Thus the effective index for TM-polarized light changes very little with the material index; i.e., it is influenced very little by the wavelength, resulting in a lower dispersion value. For cases in which the INS is composed of dispersive material and air, the maximal dispersion effect is expected to occur at a duty ratio higher than 50%, since the effect of material dispersion increases with the duty ratio, whereas the structural dispersion reaches its maximal value for $f = 0.5$.

By comparing Figs. 2 and 3, we notice that the total dispersion (both material and structural dispersions) is always larger than the structural dispersion, as expected for GaAs possessing normal dispersion.

Next, we analyze an INS composed of fused silica (having an intrinsic anomalous dispersion at the wavelength of 1.55 μm) and air. As in the previous case, the refractive index of the fused silica is calculated by the Sellmeier equation [see Eq. (33)] by use of the following parameters:[35]

$$A_1 = 0.6961663, \quad A_2 = 0.4079426, \quad A_3 = 0.8974794,$$
$$\lambda_1 = 0.0684043, \quad \lambda_2 = 0.1162414, \quad \lambda_3 = 9.896161.$$

The obtained dispersion versus the period-to-wavelength ratio is shown in Fig. 4, demonstrating that a wide range of dispersion values can be obtained. In particular, zero total dispersion can be achieved at a point at which the intrinsic material dispersion and the structural dispersion cancel each other. Owing to the relatively low index contrast between the fused silica and air, relatively low form birefringence is achieved, and the difference in dispersion terms for both polarization states is relatively small.

As shown, the structural dispersion term is always normal. However, there are cases in which one would like to generate strong anomalous dispersion within the INS. This case is analyzed in Section 4.

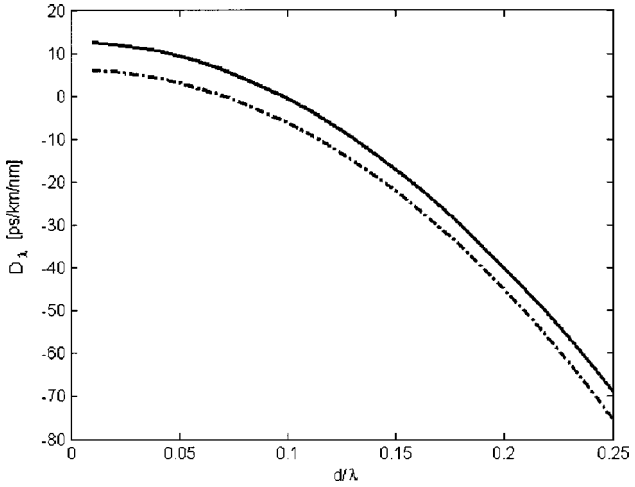

Fig. 4. Total linear dispersion coefficient versus d/λ in a fused-silica–air periodic structure (fill factor $f = 0.5$) for TE (solid curve) and TM (dashed–dotted curve) polarization states.

4. PROPAGATION OF PULSED COSINE BEAMS IN INHOMOGENEOUS NANOSTRUCTURE MEDIA

In this section we extend the discussion by evaluating the dispersion coefficient of a pulse carried by a standing cosine wave in space, propagating inside the INS. Such a beam can be described by the interference between two tilted plane waves.

We use Eqs. (8) and (15) and assume α to be fixed, i.e., not depending on the optical frequency (in practice, this can be achieved by use of a diffraction grating designed to convert a single spatial mode into ± 1 diffraction orders, producing the desired cosine wave). The dispersion coefficient is described by

$$D_\nu = \frac{1}{2\pi}\frac{\mathrm{d}^2\beta}{\mathrm{d}\nu^2} = \frac{1}{2\pi\cos(\theta)}\left\{K'' + \frac{(K')^2}{K}\left[1 - \frac{1}{\cos^2(\theta)}\right]\right\}$$
$$= \frac{1}{2\pi\cos(\theta)}\left[K'' - \frac{(K')^2}{K}\tan^2(\theta)\right], \qquad (35)$$

where $\alpha = K\sin(\theta) = \pm(2\pi n/c)\nu(c/\nu n d) = 2\pi/\Lambda$, Λ is the period of the cosine beam, and all the derivatives are taken with respect to ν. The dispersion coefficient in Eq. (30) is related to the spatial frequency α (or, equivalently, to the plane-wave tilt angle θ). A similar result can be also found in Ref. 19, for the case of a Bessel beam propagating in nonguiding media. However, since the pulse is now propagating inside the INS, the K', K'' values are influenced by both intrinsic material dispersion and structural dispersion, introducing an additional degree of freedom to the design.

Next, we re-examine the INS made of alternating GaAs and air layers for illumination with a cosine wave with the dispersion relation of Eq. (35). The dispersion coefficient is now calculated versus the plane-wave tilt angle (θ) for several period-to-wavelength ratios. As before, the

RCWA algorithm is applied over a limited wavelength span, and the propagation constant for each wavelength is determined. The refractive index can now be found with Eq. (8). The results, shown in Fig. 5, demonstrate that increasing the period-to-wavelength ratio tends to reduce the dispersion coefficient, i.e., move the dispersion curve toward normal values. On the other hand, increasing the spatial frequency of the cosine beam tends to result in an increased dispersion coefficient, i.e., move the dispersion curve toward anomalous values. These two opposite effects allow one to achieve almost any desired dispersion value. For example, by proper combination of spatial beam frequency and period-to-wavelength ratio (see Fig. 5), zero dispersion can be obtained. This is an important result, especially for INS realizations in guided-wave structures, offering a great practical potential and significance. For such a case, the spatial frequency of the cosine beam is determined mainly by the waveguide geometry, which cannot be arbitrarily chosen owing to practical constraints. One should also notice the high dispersion values of the TM polarization state at high spatial cosine frequencies. This can be explained by the large index difference. The effective refractive index of the TM state is much smaller than that of the TE, i.e., $K_{\mathrm{TM}} < K_{\mathrm{TE}}$. As α increases, it approaches K_{TM}, leading to a large propagation angle and reducing the $\cos(\theta)$ term in Eq. (35). As a result, the dispersion coefficient is significantly increased.

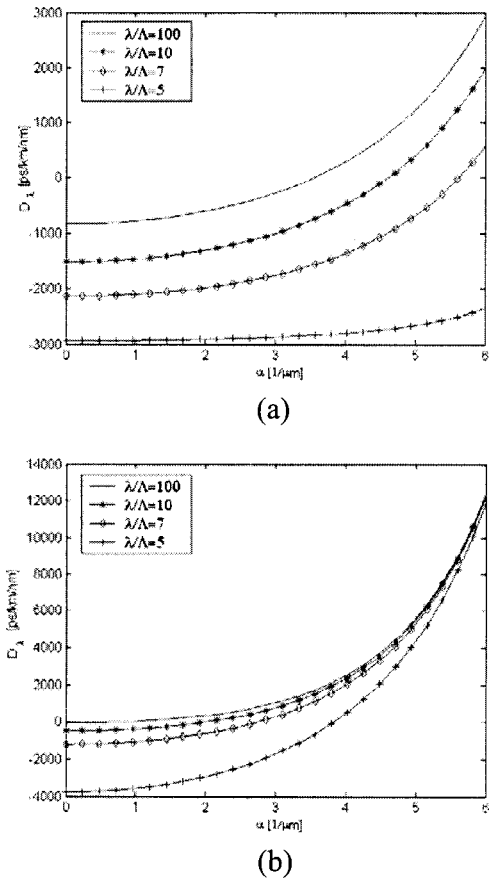

Fig. 5. Total linear dispersion coefficient versus angular frequency α in a GaAs–air periodic structure (fill factor $f = 0.5$): (a) TE polarization and (b) TM polarization.

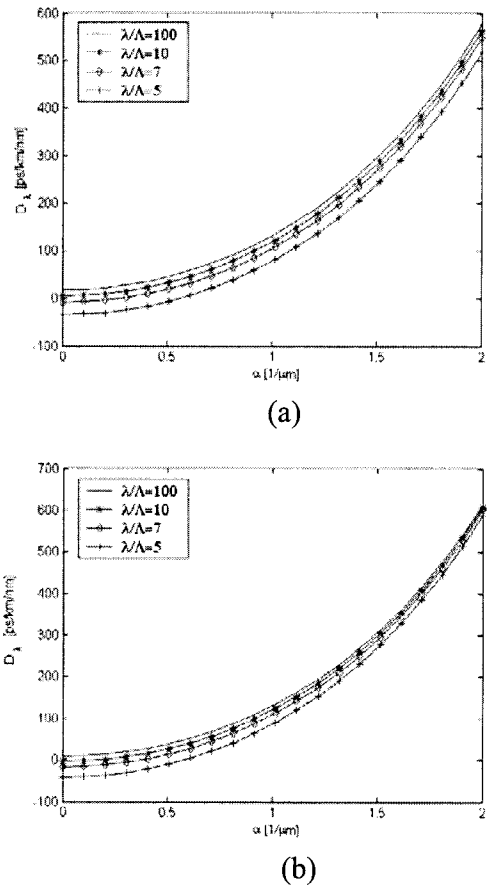

Fig. 6. Total linear dispersion coefficient versus angular frequency α in a fused-silica–air periodic structure (fill factor $f = 0.5$): (a) TE polarization and (b) TM polarization.

An additional advantage of devices made of INSs is demonstrated by reconsidering a structure made of fused silica with anomalous dispersion and air. It was shown[19] that, with materials having anomalous dispersion, the combination of waveguide-type dispersion and material dispersion cannot be combined to achieve zero dispersion, since increasing the spatial beam frequency tends to increase the anomalous dispersion. In contrast, an INS can provide compensation for such anomalous dispersion by increasing the period-to-wavelength ratio, as shown clearly in Fig. 6. By observing these results, it is evident that almost any desired dispersion value can now be obtained, including a zero-dispersion value. Moreover, there is a very large number of combinations capable of producing a specific desired dispersion value. This is considered to be a significant advantage, since it allows an additional degree of freedom in the component design. As expected, there is no major difference between the obtained results for TE and TM polarizations, owing to the relatively low birefringence ($\Delta n < 0.1$), which is the result of the low index contrast between the fused silica and air.

5. CONCLUSIONS

A novel, to our knowledge, analysis of the dispersion properties for a pulse propagating in a dielectric nonguiding media made of INSs is presented. The interaction of the

optical wave with the nanostructure provides modified dispersion characteristics. We use the term structural dispersion to explain this phenomenon. We investigate the dispersion of a pulse propagating within the INS starting by presenting the analogy between the continuum of free-space modes and the discrete waveguide modes and then by discussing two special cases of a pulse carried by a plane wave in space and a pulse carried by a standing cosine wave in space. We present an approximate analytic model capable of predicting the structural dispersion coefficient. The model is compared with more accurate results, calculated with rigorous coupled-wave analysis. RCWA is also used for the calculation of the combined dispersion coefficient, taking into account the material, structural, and waveguide-type dispersions. By taking these effects into account, it is shown that one can control the amount of the total effective dispersion to almost any extent. By using proper materials to construct the INS, one can also achieve an adaptive device, with the capability to dynamically modify the dispersion properties. It is evident that devices made of INSs can be useful for dispersion management and dispersion control applications, with an additional advantage of allowing monolithic integration with other components into a system on a chip.

ACKNOWLEDGMENTS

This research is supported in part by the U. S. Air Force Office of Scientific Research, the National Science Foundation, the Defense Advanced Research Projects Agency, and the Space and Naval Warfare Systems Command. Uriel Levy acknowledges the Yad Ha-Nadiv fund for financial support (Rothschild fellowship).

Uriel Levy, the corresponding author, can be reached by e-mail at ulevy@ece.ucsd.edu.

REFERENCES

1. I. M. Nisoli, S. De Silvestri, O. Svelto, R. Szipocs, K. Ferencz, C. Spielmann, S. Sartania, and F. Krausz, "Compression of high-energy laser pulses below 5 fs," Opt. Lett. **22**, 522–524 (1997).
2. I. P. Bilinsky, J. G. Fujimoto, J. N. Walpole, and L. J. Missaggia, "Semiconductor-doped-silica saturable-absorber films for solid-state laser mode locking," Opt. Lett. **23**, 1766–1768 (1998).
3. U. Morgner, F. X. Kartner, S. H. Cho, Y. Chen, H. A. Haus, J. G. Fujimoto, E. P. Ippen, V. Scheuer, G. Angelow, and T. Tschudi, "Sub-two-cycle pulses from a Kerr-lens mode-locked Ti:sapphire laser," Opt. Lett. **24**, 411–413 (1999).
4. D. H. Sutter, G. Steinmeyer, L. Gallmann, N. Matuschek, F. M. Genoud, U. Keller, V. Scheuer, G. Angelow, and T. Tschudi, "Semiconductor saturable-absorber mirror-assisted Kerr-lens mode-locked Ti:sapphire laser producing pulses in the two-cycle regime," Opt. Lett. **24**, 631–633 (1999).
5. F. Qeullen, "Dispersion cancellation using linearly chirped Bragg grating filters in optical waveguides," Opt. Lett. **12**, 847–849 (1987).
6. A. J. Antos and D. K. Smith, "Design and characterization of dispersion compensating fiber based on the LP_{01} mode," J. Lightwave Technol. **12**, 1739–1745 (1994).
7. G. P. Agrawal, *Fiber-Optic Communication Systems* (Wiley, New York, 1992).
8. D. Mendlovic, Z. Zalevsky, and P. Andreas, "A novel device for achieving negative or positive dispersion and its applications," Optik (Stuttgart) **110**, 45–50 (1999).
9. C. K. Madsen, G. Lenz, T. N. Nielsen, A. J. Bruce, M. A. Cappuzzo, and L. T. Gomez, "Integrated optical all pass filters for dispersion compensation," in *WDM Components*, D. A. Nolan, ed., Vol. 29 of OSA Trends in Optics and Photonics Series (Optical Society of America, Washington, D.C., 1999), pp. 142–149.
10. K. Djordjev, S.-J. Choi, S.-J. Choi, and P. D. Dapkus, "Study of the effects of the geometry on the performance of vertically coupled InP microdisk resonators," J. Lightwave Technol. **20**, 1485–1492 (2002).
11. I. Kaminow and T. Li, *Optical Fiber Telecommunications IV*, 4th ed. (Academic, San Diego, Calif., 2002), Part B, pp. 642–724.
12. B. E. A. Saleh and M. C. Teich, *Fundamentals of Photonics* (Wiley, New York, 1991), pp. 182–191.
13. M. A. Porras, R. Borghi, and M. Santarsiero, "Few-optical-cycle Bessel–Gauss pulsed beams in free space," Phys. Rev. E **62**, 5729–5737 (2000).
14. M. A. Porras, "Diffraction-free and dispersion-free pulsed beam propagation in dispersive media," Opt. Lett. **26**, 1364–1366 (2001).
15. J. Lu and J. F. Greenleef, "Nondiffracting X waves—exact solutions to free space scalar wave equation and their finite aperture realization," IEEE Trans. Ultrason. Ferroelectr. Freq. Control **39**, 19–31 (1992).
16. Z. Y. Liu and D. Y. Fan, "Propagation of pulsed zeroth-order Bessel beams," J. Mod. Opt. **45**, 17–21 (1998).
17. C. J. R. Sheppard, "Bessel pulse beams and focus wave modes," J. Opt. Soc. Am. A **18**, 2594–2600 (2001).
18. W. Hu and H. Guo, "Ultrashort pulsed Bessel beams and spatially induced group-velocity dispersion," J. Opt. Soc. Am. A **19**, 49–53 (2002).
19. B. Lu and Z. Liu, "Propagation properties of ultrashort pulsed Bessel beams in dispersive media," J. Opt. Soc. Am. A **20**, 582–587 (2003).
20. I. Richter, P. C. Sun, F. Xu, and Y. Fainman, "Design considerations of form birefringent microstructures," Appl. Opt. **34**, 2421–2429 (1995).
21. F. Xu, R. Tyan, P. C. Sun, C. Cheng, A. Scherer, and Y. Fainman, "Fabrication, modeling, and characterization of form-birefringent nanostructures," Opt. Lett. **20**, 2457–2459 (1995).
22. R. Tyan, P. C. Sun, A. Scherer, and Y. Fainman, "Polarizing beam splitter based on the anisotropic spectral reflectivity characteristic of form-birefringent multilayer gratings," Opt. Lett. **21**, 761–763 (1996).
23. R. Tyan, A. Salvekar, Cheng, A. Scherer, F. Xu, P. C. Sun, and Y. Fainman, "Design, fabrication, and characterization of form-birefringent multilayer polarizing beam splitter," J. Opt. Soc. Am. A **14**, 1627–1636 (1997).
24. F. Xu, R. Tyan, P. C. Sun, Y. Fainman, C. Cheng, and A. Scherer, "Form-birefringent computer-generated holograms," Opt. Lett. **21**, 1513–1515 (1996).
25. D. L. Brundrett, E. N. Glytsis, and T. K. Gaylord, "Subwavelength transmission grating retarders for use at 10.6 μm," Appl. Opt. **35**, 6195–6202 (1996).
26. S. M. Rytov, "Electromagnetic properties of a finely stratified medium," Sov. Phys. JETP **2**, 466–475 (1956).
27. M. G. Moharam and T. K. Gaylord, "Rigorous coupled-wave analysis of planar grating diffraction," J. Opt. Soc. Am. **71**, 811–818 (1981).
28. A. Taflove and S. Hagness, *Computational Electrodynamics: the Finite-Difference Time-Domain Method* 2nd ed. (Artech House, Norwood, Mass., 2000).
29. D. W. Parther, M. S. Mirotznik, and J. N. Mait, "Boundary integral methods applied to the analysis of diffractive optical elements," J. Opt. Soc. Am. A **14**, 34–43 (1997).
30. K. D. Paulsen, "Finite-element solution of Maxwell's equations with Helmholtz forms," J. Opt. Soc. Am. A **11**, 1434–1444 (1994).
31. H. Kikuta, Y. Ohira, and K. Iwata, "Achromatic quarter-wave plates using the dispersion of form birefringence," Appl. Opt. **36**, 1566–1572 (1997).

32. G. Nordin and P. Deguzman, "Broadband form birefringent quarter-wave plate for the mid-infrared wavelength region," Opt. Express **5**, 163–168 (1999).
33. T. A. Birks, D. Mogilevtsev, J. C. Knight, and P. St. J. Russell, "Dispersion compensation using single-material fibers," IEEE Photon. Technol. Lett. **11**, 674–676 (1999).
34. J. Goodman, *Introduction to Fourier Optics*, 2nd ed. (McGraw-Hill, New York, 1996).
35. C. Gu and P. Yeh, "Form birefringence dispersion in periodic layered media," Opt. Lett. **21**, 504–506 (1996).
36. M. Bass, E. W. V. Stryland, D. R. Williams, and W. L. Wolfe, *Handbook of Optics*, 2nd ed. (McGraw-Hill, New York, 1995), Chap. 33, pp. 26, 33, 63, and 69.
37. W. Nakagawa, R. C. Tyan, P. C. Sun, F. Xu, and Y. Fainman, "Ultrashort pulse propagation in near-field periodic diffractive structures by use of rigorous coupled-wave analysis," J. Opt. Soc. Am. A **18**, 1072–1081 (2001).